Title

Progression of Parkinson's disease pathology is reproduced by intragastric administration of rotenone in mice

Authors and Affiliations

Francisco Pan-Montojo[1,2,*], Oleg Anichtchik[3], Yanina Dening[1], Lilla Knels[1], Stefan Pursche[4], Roland Jung[5], Gabriele Gille[2], Maria Grazia Spillantini[3], Heinz Reichmann[2] and Richard H.W. Funk[1,*]

[1]*Institute of Anatomy, Medical Faculty Carl Gustav Carus, Dresden University of Technology, Fetscherstr. 74, 01307 Dresden, Germany*

[2]*Dept. of Neurology, Medical Faculty Carl Gustav Carus, Dresden University of Technology, Fetschertr. 74, 01307 Dresden, Germany*

[3]*Center for Brain Repair, University of Cambridge, E.D. Adrian Building, Forvie Site, Robinson Way, Cambridge CP2 0PY, United Kingdom*

[4]*Dept. of Internal Medicine I, Medical Faculty Carl Gustav Carus, Dresden University of Technology, Fetscherstr. 74, 01307 Dresden, Germany*

[5]*Experimental Center, Medical Faculty Carl Gustav Carus, Dresden University of Technology, Fetscherstr. 74, 01307 Dresden, Germany*

** Corresponding authors: Francisco J. Pan-Montojo and Richard H.W. Funk, Institut für Anatomie, Medizinische Fakultät Carl Gustav Carus, TU Dresden, Fetscherstr. 74, 10307 Dresden, Germany. e-mail: pan-montojo@mpi-cbg.de and richard.funk@tu-dresden.de*

Abstract

In Parkinson's disease patients pathology follows a characteristic pattern involving *inter alia* the enteric nervous system, the dorsal motor nucleus of the vagus, the intermediolateral nucleus of the spinal cord and the substantia nigra, providing the basis for the neuropathological staging of the disease. Here we report that intragastrically administered rotenone, a commonly used pesticide that inhibits mitochondrial Complex I, is able to reproduce PD pathological staging as found in patients. Our results show that low doses of chronically and intragastrically administered rotenone induce PD pathology in all the above-mentioned nervous system structures in wild-type mice. Interestingly, HPLC analysis showed no

rotenone levels in the systemic blood or the central nervous system (CNS) (detection limit [rotenone]<20nM), suggesting that rotenone is detoxified by the liver. These alterations are sequential, appearing only in synaptically connected nervous structures, treatment time-dependent and accompanied by inflammatory signs and motor dysfunctions. These results strongly suggest that the local effect of pesticides on the ENS might be sufficient to induce PD progression and to reproduce the neuroanatomical and neurochemical features of PD staging. Thus, providing new insight into how environmental factors could trigger PD and suggesting a transsynaptic mechanism by which PD might propagate to and through the CNS.
.

Introduction

Parkinson´s Disease (PD) is a highly prevalent disease affecting 0.3% of the general population and 1-3% of the population over the age of 65 . Slowly progressive, PD is characterized by dysfunctions of the somatomotor system (i.e., rigidity, bradykinesia, postural instability, gait dysfunction and tremor) usually dominating the clinical picture of sporadic PD . Main symptoms are caused by the progressive degeneration of the nigrostriatal dopaminergic pathway These complaints, however, are often preceded or accompanied by other symptoms that also emerge during the disease course . Hyposmia and gastrointestinal alterations are among the non-motor signs that develop early, often preceding motor symptoms by years , and are normally accompanied by autonomic dysfunction as well as the experience of pain .

A pathological hallmark of PD is the accumulation of filamentous, cytoplasmic inclusions consisting mainly of alpha-synuclein aggregations in the form of Lewy bodies (LB) or Lewy neurites (LN) . They are found in certain areas of the central nervous system (CNS) (e.g. dorsal motor nucleus of the vagus (DMV), intermediolateral nucleus in the spinal cord (IML), the locus coeruleus (LC) and the olfactory bulb (OB)) and the peripheral nervous system (PNS) (caeliac ganglia and ENS) of PD patients . These pathological findings are usually associated with an inflammatory response and phosphorylation of alpha-synuclein (Ser129) that accumulates as a component of LB in the brains of patients with alpha-synucleinopathies .

Although genetic mutations contribute to the development of rare familial forms of PD (i.e. mutations in alpha-synuclein, Parkin, LRRK2, PINK1 genes) most of the cases are sporadic and due to unclear aetiologies. It has been postulated that mitochondrial

dysfunction , oxidative stress , inflammatory response and protein mishandling may play an important role in sporadic PD pathogenesis . On the other hand, multiple epidemiological studies suggest an association between pesticides and PD incidence .

Many studies have used different pesticides and routes of administration in order to reproduce pathological and clinical findings of PD in animals . These models show different combinations of PD clinical and pathological features like selective decrease in TH-positive neurons, presence of LB in the SN, impaired striatal dopaminergic innervation or motor dysfunctions. Nevertheless, they fail to reproduce the complete spectrum of pathological disease progression and provide little information on the risk of environmental exposure because these methods bypass the physical and metabolic defences of the organism. Moreover, systemic administration of rotenone in C57BL/6J mice has failed to reproduce any of PD pathological findings .

Braak and colleagues have suggested that the pathological process starts in the ENS and OB progressing into the CNS through anatomically connected structures . Therefore, in order to investigate the effect of ingested pesticides on the ENS and its possible role in PD pathological progression, we administered rotenone intragastrically to one-year old mice using a gastric tube.

Results

In order to test whether the local effect on the ENS of an orally administered pesticide could reproduce this progression, we decided to administer rotenone intragastrically to one-year old mice using a gastric tube.

Before starting the experiments and to ensure that rotenone was detoxified by the liver not reaching the systemic blood or the CNS, we performed HPLC analysis on blood, brain and brainstem samples of non-experimental C57BL/6J mice. Blood was extracted from 8 weeks-old mice treated with 2.5, 5, 10 and 20 mg/kg rotenone for one week. Brain and brainstem samples were obtained from one-year old mice treated with 5, 10 and 20 mg/kg rotenone for 5 days. We were unable to detect rotenone via HPLC in the blood at doses of 5 mg/kg or lower and in the brainstem or brain at doses of 10 mg/kg or lower (supplementary Fig. 1). Therefore, we decided to use a dose of 5 mg/kg rotenone to treat experimental mice. HPLC analysis made on weeks 2, 4 and 10 of treatment showed the same results (data not shown).

Rotarod test

We performed an accelerating protocol of the rotarod test, that provides a more discriminative way to correlate motor deficits against lesion size to investigate whether treated mice also showed motor dysfunctions. Rotarod test results showed a significant difference ($p<0.05$) in the task performance in 3 but not 1.5 months treated mice when compared to controls at an acceleration of 0.3 but not 0.2 rpm/sec (supplementary Fig. 1).

After PFA perfusion various immunohistochemistry techniques were used to analyse whether the ENS, the IML, the DMV or the SN were affected in our mouse model and if these alterations were progressive.

Effects of rotenone on the ENS

We detected alpha-synuclein in duodenum and ileum ENS neurons from both control and treated animals. However, distribution, inclusion number and amount of alpha-synuclein differed between treated and control animals. Control mice showed alpha-synuclein mainly in the periphery of the neuronal soma (Fig. 1A) while in treated mice alpha-synuclein was increased and present both inside and outside the neural soma (Fig. 1B), with larger alpha-synuclein accumulations (∅>6 µm) in 20% of the analyzed ganglia after 3 months treatment (Fig. 1C). To investigate whether alpha-synuclein was aggregated, we double stained with alpha-synuclein and Thioflavine-S, a substance that recognises filamentous aggregates. We observed alpha-synuclein aggregation only in the larger accumulations from three months treated mice (Fig. 1D). Associated alpha-synuclein phosphorylation and gliosis was confirmed by the presence of GFAP and Ser-129 phosphorylated alpha-synuclein in ENS ganglia from treated (Fig. 1H and 1J) but not control mice (Fig. 1G and 1I). Immunohistochemistry for alpha-synuclein using an alternative alpha-synuclein antibody (Syn-1) confirmed the presence of synuclein staining within ganglia of ENS. No specific staining with AT8 antibody (phosphorylated tau marker) was detected and control immunostaining with secondary antibodies showed no unspecific staining.

Image analysis using Image J Software showed that the total surface stained with alpha-synuclein inside the ganglia and the number of inclusions significantly increased after 1.5 months rotenone treatment when compared to control both in duodenum and ileum ($p<0.01$) (Fig. 1E and 1F). Interestingly, the value of these parameters decreased after 3 months treatment coinciding with the appearance of larger inclusions of aggregated alpha-synuclein (Fig. 1C).

Oxidative damage in the ENS leads to alpha-synuclein accumulation in the IML and the DMV

Next, we wanted to determine whether the local effect of rotenone on the ENS could lead to alterations in the synaptically connected structures, the IML and the DMV. Indeed, we observed PD related pathological changes in both sites. We observed an increase in alpha-synuclein and some large alpha-synuclein intracellular inclusions (2% of the analyzed images) in $ChAT^+$ neurons of the intermediolateral nucleus of the spinal cord (IML) (∅>7.5 µm) (Fig. 2B and 2C) as well as increased alpha-synuclein staining in the dorsal horn layer I after 1.5 and 3 months treatment (Fig 2G and 2H). We used image analysis to quantify alpha-synuclein increase by measuring fluorescence in the IML. Fluorescence measurements showed that the IML/IML adjacent region ratio of alpha-synuclein mean fluorescence intensity was increased in both 1,5 ($p<0.01$) and 3 weeks-treated mice ($p<0.01$) when compared to controls (Fig. 3D-F). Thus suggesting an alpha-synuclein increase in preganglionic sympathetic neuron processes. This difference was not observed in $ChAT^+$ motor neurons of the anterior horn (supplementary Fig. 2). These results were confirmed by immunohistochemistry on DAB stained sections, where the intensity of alpha-synuclein staining was greater in the tissues of 3 months treated animals when compared to control sections (supplementary Fig. 2). Interestingly, we noticed no differences in GFAP staining between treated and control mice in this area (data not shown).

In the dorsal motor nucleus of the vagus (DMV), 1.5 and 3 months rotenone treatment resulted in increased intracellular alpha-synuclein accumulation inside $ChAT^+$ neurons (Fig. 3B) when compared to controls. We also observed an inflammatory associated reaction, with increased GFAP and some activated microglial cells around neurons of the DMV in treated but not control mice (Fig. 3G and 3H). Remarkably, $ChAT^+$ neurons from adjacent hypoglossus nuclei showed neither alpha-synuclein accumulations nor GFAP increase (data not shown). Control immunostaining with secondary antibodies showed auto-fluorescent inclusions inside DMV neurons from treated mice (Fig. 3C). Previous studies have identified auto fluorescent inclusions as lipofuscin accumulations . Lipofuscin granules mainly contain lipids. Therefore, we used Sudan IV staining, confirming them as lipofuscin inclusions (data not shown). In order to avoid auto-fluorescence interference, we also performed immunohistochemistry with DAB detection of alpha-synuclein on 1.5 and 3 months treated mice. This technique also showed alpha-synuclein accumulation in DMV neurons when compared to controls (Fig. 3D-F). Alpha-synuclein was detected in both, neurons and the neuropil, however only in treated animals the staining of neural processes was visible (Fig. 3F). These results suggest that both directly synaptically connected (DMV) and indirectly synaptically connected (IML) structures are affected by the alterations produced in the ENS by rotenone.

Alpha-synuclein pathology progresses into the SN after three months orally rotenone treatment

In order to investigate whether other CNS structures related to PD were affected, we analyzed the SN and the striatum. In the SN, we observed an increased intracellular alpha-synuclein (Fig. 4B) together with larger alpha-synuclein accumulations in the SNc (Fig. 4c) and a significant ($p<0,05$) decrease in the number of TH^+ neurons (Fig. 4D) in 3 but not 1.5 month treated mice when compared to controls (Fig. 4A).). Remarkably, we did not observe significant differences in dopaminergic innervation of the striatum (Fig. 4E-F), brain tau protein, lipofucsin granules or alpha-synuclein accumulation in other brain areas (e.g. cerebellum, cortex or striatum) (data not shown) between treated and control animals at any time-point..

Discussion

It has been proposed that the PD-related inclusion body pathology in the nervous system progresses in six stages, starting at the OB and the ENS and affecting closely connected nerval sites . Interestingly, both the OB and the ENS are the only nervous system structures directly exposed to environmental substances. On the other hand, recent reports on patients with PD who received transplants of embryonic mesencephalic neurons show that in some cases, mesencephalic neurons grafted into the striatum of PD patients develop both alpha-synuclein and ubiquitin positive LB . According to these and other evidences , Brundin and colleagues proposed inflammation, oxidative stress, excitotoxicity, prion-disease-like mechanisms and loss of neurotrophic support as possible underlying mechanisms for PD propagation .

Recently developed PD animal toxic models fail to reproduce the entire pathological spectrum of the disease. Moreover, they also avoid the important physiological defence mechanisms to external substances .

Our results show that chronic treatment with intragastrically administered rotenone reproduces all PD reported pathological features in the above-mentioned nervous system structures. Interestingly, these alterations occur without significant levels of the pesticide in the blood [rotenone]<20nM or the CNS [rotenone]<<20nM (as we didn't detect it even in 10 mg/kg treated mice, see Results). We observed alpha-synuclein accumulation and phosphorylation, inflammatory signs and loss of nigral TH^+ neurons in our treated mice. Moreover, we also observed intracellular auto-fluorescent Sudan-IV^+ lipofuscin inclusions. Lipofuscin has been considered a biomarker for oxidative stress and its presence suggests an increase in oxidative stress and accumulation of advanced glycation

end products . The inflammation pattern observed indicates that inflammation is not involved in the propagation of the alteration but is perhaps a consequence of neuronal damage or alpha-synuclein accumulation *in situ*. Remarkably, there was specificity in the nervous structures affected and only neuronal subpopulations synaptically connected showed alterations while nearby areas remained unaffected. We did not observe any alterations in the OB, striatal TH or brain tau protein levels as reported in other rotenone models , suggesting greater selectivity of the neuronal damage in our model. Finally, we also observed differences in the rotarod test performance. Interestingly this difference was only observed after 3 months treatment together with SN impairment. However, these results are difficult to interpret, as it is very unlikely that neuronal loss in the sustantia nigra alone without a reduction in striatal dopamine could be responsible for these alterations. Unfortunately, the little amount of tissue available did not allow us to measure dopamine levels in the striatum of treated mice. Although further mechanistic studies are necessary (i.e. strategically-placed nervous system lesions), these results strongly support an enteric nervous system spread hypothesis. The selectivity of the neuronal affection together with the low blood and CNS rotenone levels make us speculate with the possibility of a transsynaptic mechanism being responsible for this remarkable pattern of progression. It might be argued that by HPLC undetectable levels of rotenone in the blood could induce this pattern but the results from other studies using animal models with higher systemic concentrations of rotenone speak against this possibility. Richter and colleagues have shown that subcutaneous administration of 2.5-4 mg/kg of rotenone for 30-40 days does not induce striatal degeneration or neuronal loss in the CNS of C57BL/6J mice. On the other hand, Betarbet and colleagues observed striatum degeneration before SN affection with the lowest dose (2,5 mg/kg) and treatment time (7 days) of systemically administered rotenone in rats, suggesting greater sensibility of striatal nerve terminals. Remarkably, they did not observe degeneration anywhere else in the CNS. To our knowledge, this is the first animal model able to reproduce the full spectrum and progression of PD pathology. Therefore, we strongly believe that this new animal model of the disease provides a better tool for understanding of the mechanisms underlying PD's pathophysiology and may suggest novel pathways for the therapeutic intervention.

Materials and Methods

3.1 Animal procedures. One-year old C57BL/6J mice (Janvier, France) were housed at room temperature under a 12-h light/dark cycle. Food and water was provided *ad libitum*. Mice were divided in four groups (n=5) and treated 5 days a week for 1.5 and 3 months. A stomach tube was used to administer 0.01 ml/g animal weight of rotenone solution

(0.625 mg/ml rotenone (Sigma-Aldrich, Germany), 4% carboxymethylcellulose (Sigma-Aldrich, Germany) and 1.25% chloroform (Carl Roth, Germany)) corresponding to a 5 mg/kg dose. Controls were treated only with the vehicle (4% carboxymethylcellulose and 1.25% chloroform). Blood extraction for High Performance Liquid Chromatography (HPLC) analysis was obtained from the retina plexus using a glass capilar under general anesthesia (0.01 ml/g of Ketamin i.p.). CNS-tissue was obtained after cervical dislocation. All animal experiments were carried out in accordance with the National Institutes of Health Guide for the Care and Use of Laboratory Animals, and protocols were approved by the Saxonian Committee for Animal Research, Germany.

2.2 Measurement of rotenone levels in mice plasma and CNS. Blood from control and 2.5, 5, 10 and 20 mg/kg 8 weeks-old one-week treated mice (n=3) was extracted 1, 2 and 3 hours after rotenone administration and pooled in the same tube. Serum samples were obtained by centrifugation at 3000 rpm (Micro 12-24, Hettich Zentrifugen, Germany). Serum was analysed using a modified HPLC protocol as previously described . Brain and brainstem from control, 5 (n=3), 10 (n=3) and 20 mg/kg (n=1) rotenone 5 day-treated one-year old animals were collected 1 and 3 hours after the last rotenone administration and processed as already described by others . The methods were linear over a concentration range from 10 to 500 ng/ml, the interassay precision expressed as coefficient of variation was <10%. The limit of detection was 10 ng/ml.

2.3. Immunohistochemistry. Immunofluorescence was performed on 40 µm (brain and spinal cord) and 20 µm (gastrointestinal tract) paraformaldehyde fixed frozen sections. Non specific background staining from CNS sections was blocked overnight at 4°C in blocking solution (5% donkey serum (Jackson Immunoresearch Laboratories), 0.4% Triton-X-PBS), whereas gut sections were blocked for two hours at room temperature (RT) using 5% donkey serum in 0.25% Triton-X-PBS. Sections were then incubated with the primary antibodies for 24 hours at 4°C, washed in PBS, incubated for one hour at RT with the fluorescent secondary antibodies, washed in PBS again and mounted using Vectashield® mounting medium for fluorescence with DAPI (Vectro Laboratories, USA). The following polyclonal primary antibodies were used: goat anti-ChAT (1:500, Chemicon, USA), sheep anti-TH (1:1000, Peel freeze), rabbit anti-alpha-synuclein (1:400, Santa Cruz, USA); chicken anti-GFAP (1:1000, Abcam, UK) and rat anti-MHC II clone M5/114.15.2 (1:200, BD Pharmigen, CA, USA), rabbit anti-phospho-alpha-synuclein (phospho S129) (1:50, Abcam, UK), chicken anti-ßIII-tubulin (1:500, Novus Biologicals, USA). These were coupled with the following secondary antibodies: Alexa® 488 donkey anti-rabbit, Alexa® 488 donkey anti-goat, Alexa®488 donkey anti-rat, Alexa® 555 and Alexa®594 donkey anti-sheep and donkey anti-goat (all 1:500 and from Invitrogen, USA) and 647 donkey anti-chicken (1:200, Jackson Immunoresearch

Laboratories, USA). DAB immunohistochemistry was done as reported before . Mouse anti alpha-synuclein (BD Transduction Laboratores, San Jose, CA USA) or AT8 (Pierce Biotechnology, Rockford, IL USA) primary antibodies were used at 1:1,000.

2.4. Imaging. Immunostained sections were analysed using Leica Leitz DMRD bright field microscope and a Zeiss confocal microscope (LSM 510, Carl Zeiss, Jena). Z-stacks from immunofluorescence gut sections were obtained using an Apo-63X objective. A Z-stack was acquired for 7 consecutive ganglia per gut section/animal, with 1µm spacing in the Z-direction. The optical resolution limit for these images was 0,13 µm in the XY direction and 1 µm in the Z direction. Single images of the IML from spinal cord sections were acquired using the same microscope equipped with an Apo-25X objective. The optical resolution limit for these images was 0,48 µm in the XY direction. No additional post-acquisition manipulations of digital images were done. Digital images were then processed using ImageJ free software (Rasband, W.S., ImageJ, U. S. National Institutes of Health, Bethesda, Maryland, USA, http://rsb.info.nih.gov/ij/, 1997-2005), where only cropping of the original image and minor adjustment of the brightness and contrast were performed.

2.5. Image analysis. Immunofluorescence image analysis was made using ImageJ and performed by a third independent researcher, unaware of images origin. Z-stacks from gut sections were used for quantifying the alpha-synuclein droplet size. For each stack, the ganglion region was selected and isolated. Automatic segmentation of alpha-synuclein droplets was made using an entropy-based thresholding method, and operations on binary images. The in-focus plane for alpha-synuclein droplets was then searched for, by identifying the plane where droplet total surface was maximal. This sole plane was used for further analysis. The total alpha-synuclein surface and inclusion number were measured and normalized by ganglion/neuron area for statistical analyses. IML images were used to compute a fluorescence ratio, by normalizing the alpha-synuclein signal in the IML region by that of adjacent areas.

2.6. Stereological procedures. Every sixth section was stained against TH and alpha-synuclein and used for stereological analysis. The number of TH^+ neurons in the SN was estimated using the Optical Fractionator principle with StereoInvestigator software (MicroBrightField Inc., Williston, USA) on a Zeiss Axioplan microscope and using a 20X objective. Total TH^+ neuron number (N) was calculated using the formula N 1/4 SQ– · (t h) · (1 asf) · 1 ssf, where Q– 1/4 is the total number of cells counted, t 1/4 is the section thickness, h 1/4 is the height of optical disector, asf 1/4 is the area of sampling fraction 1/4 a(frame) a(x,y step) and ssf 1/4 is the section sampling fraction.

2.7. Statistical analysis. All data was tested for significance using two-way ANOVA, significance being $p \leq 0.05$.

Acknowledgments

Acknowledgements: We thank C.-P. Heisenberg and G.A. O'Sullivan for critical reading of the manuscript. G. Kempermann and A. Garthe for the rotarod equipment. H. Braak, M. Zerial, E. Tanaka, M. Rodrigo, A. Storch, M. Kamal, A. Hermann and H. Rohrer for stimulating scientific discussion. C. Nipproschke, S. Kanzler, A. Böhme, P. Lorenz and E. Fineberg for technical assistance.

References

1. de Rijk MC, Launer LJ, Berger K, Breteler MM, Dartigues JF, et al. (2000) Prevalence of Parkinson's disease in Europe: A collaborative study of population-based cohorts. Neurologic Diseases in the Elderly Research Group. Neurology 54: S21-23.
2. Litvan I, Bhatia KP, Burn DJ, Goetz CG, Lang AE, et al. (2003) Movement Disorders Society Scientific Issues Committee report: SIC Task Force appraisal of clinical diagnostic criteria for Parkinsonian disorders. Mov Disord 18: 467-486.
3. Crossman AR (1989) Neural mechanisms in disorders of movement. Comp Biochem Physiol A Comp Physiol 93: 141-149.
4. Albin RL, Young AB, Penney JB (1989) The functional anatomy of basal ganglia disorders. Trends Neurosci 12: 366-375.
5. Lang AE, Obeso JA (2004) Time to move beyond nigrostriatal dopamine deficiency in Parkinson's disease. Ann Neurol 55: 761-765.
6. Chaudhuri KR, Martinez-Martin P (2008) Quantitation of non-motor symptoms in Parkinson's disease. Eur J Neurol 15 Suppl 2: 2-7.
7. Adler CH, Thorpy MJ (2005) Sleep issues in Parkinson's disease. Neurology 64: S12-20.
8. Abbott RD, Petrovitch H, White LR, Masaki KH, Tanner CM, et al. (2001) Frequency of bowel movements and the future risk of Parkinson's disease. Neurology 57: 456-462.
9. Ross GW, Abbott RD, Petrovitch H, Tanner CM, Davis DG, et al. (2006) Association of olfactory dysfunction with incidental Lewy bodies. Mov Disord 21: 2062-2067.
10. Ponsen MM, Stoffers D, Booij J, van Eck-Smit BL, Wolters E, et al. (2004) Idiopathic hyposmia as a preclinical sign of Parkinson's disease. Ann Neurol 56: 173-181.
11. Hawkes CH, Shephard BC, Daniel SE (1999) Is Parkinson's disease a primary olfactory disorder? Qjm 92: 473-480.
12. Pfeiffer RF (2003) Gastrointestinal dysfunction in Parkinson's disease. Lancet Neurol 2: 107-116.
13. Goldstein DS (2006) Orthostatic hypotension as an early finding in Parkinson's disease. Clin Auton Res 16: 46-54.

14. Goetz CG, Tanner CM, Levy M, Wilson RS, Garron DC (1986) Pain in Parkinson's disease. Mov Disord 1: 45-49.
15. Buzas B, Max MB (2004) Pain in Parkinson disease. Neurology 62: 2156-2157.
16. Spillantini MG, Schmidt ML, Lee VM, Trojanowski JQ, Jakes R, et al. (1997) Alpha-synuclein in Lewy bodies. Nature 388: 839-840.
17. Duda JE, Lee VM, Trojanowski JQ (2000) Neuropathology of synuclein aggregates. J Neurosci Res 61: 121-127.
18. Zarow C, Lyness SA, Mortimer JA, Chui HC (2003) Neuronal loss is greater in the locus coeruleus than nucleus basalis and substantia nigra in Alzheimer and Parkinson diseases. Arch Neurol 60: 337-341.
19. Wakabayashi K, Takahashi H, Ohama E, Ikuta F (1990) Parkinson's disease: an immunohistochemical study of Lewy body-containing neurons in the enteric nervous system. Acta Neuropathol 79: 581-583.
20. Forno LS (1996) Neuropathology of Parkinson's disease. J Neuropathol Exp Neurol 55: 259-272.
21. Braak H, de Vos RA, Bohl J, Del Tredici K (2006) Gastric alpha-synuclein immunoreactive inclusions in Meissner's and Auerbach's plexuses in cases staged for Parkinson's disease-related brain pathology. Neurosci Lett 396: 67-72.
22. McGeer PL, McGeer EG (2008) The alpha-synuclein burden hypothesis of Parkinson disease and its relationship to Alzheimer disease. Exp Neurol 212: 235-238.
23. Fujiwara H, Hasegawa M, Dohmae N, Kawashima A, Masliah E, et al. (2002) alpha-Synuclein is phosphorylated in synucleinopathy lesions. Nat Cell Biol 4: 160-164.
24. Paisan-Ruiz C, Jain S, Evans EW, Gilks WP, Simon J, et al. (2004) Cloning of the gene containing mutations that cause PARK8-linked Parkinson's disease. Neuron 44: 595-600.
25. Kitada T, Asakawa S, Hattori N, Matsumine H, Yamamura Y, et al. (1998) Mutations in the parkin gene cause autosomal recessive juvenile parkinsonism. Nature 392: 605-608.
26. Polymeropoulos MH, Lavedan C, Leroy E, Ide SE, Dehejia A, et al. (1997) Mutation in the alpha-synuclein gene identified in families with Parkinson's disease. Science 276: 2045-2047.
27. Schapira AH (2004) Disease modification in Parkinson's disease. Lancet Neurol 3: 362-368.
28. Jenner P (2003) Oxidative stress in Parkinson's disease. Ann Neurol 53 Suppl 3: S26-36; discussion S36-28.
29. McGeer PL, McGeer EG (2004) Inflammation and neurodegeneration in Parkinson's disease. Parkinsonism Relat Disord 10 Suppl 1: S3-7.

30. Greenamyre JT, Betarbet R, Sherer TB (2003) The rotenone model of Parkinson's disease: genes, environment and mitochondria. Parkinsonism Relat Disord 9 Suppl 2: S59-64.
31. Gorell JM, Johnson CC, Rybicki BA, Peterson EL, Richardson RJ (1998) The risk of Parkinson's disease with exposure to pesticides, farming, well water, and rural living. Neurology 50: 1346-1350.
32. Bove J, Prou D, Perier C, Przedborski S (2005) Toxin-induced models of Parkinson's disease. NeuroRx 2: 484-494.
33. Richter F, Hamann M, Richter A (2007) Chronic rotenone treatment induces behavioral effects but no pathological signs of parkinsonism in mice. J Neurosci Res 85: 681-691.
34. Monville C, Torres EM, Dunnett SB (2006) Comparison of incremental and accelerating protocols of the rotarod test for the assessment of motor deficits in the 6-OHDA model. J Neurosci Methods 158: 219-223.
35. Porta EA (2002) Pigments in aging: an overview. Ann N Y Acad Sci 959: 57-65.
36. Braak H, Sastre M, Bohl JR, de Vos RA, Del Tredici K (2007) Parkinson's disease: lesions in dorsal horn layer I, involvement of parasympathetic and sympathetic pre- and postganglionic neurons. Acta Neuropathol 113: 421-429.
37. Braak H, Rub U, Gai WP, Del Tredici K (2003) Idiopathic Parkinson's disease: possible routes by which vulnerable neuronal types may be subject to neuroinvasion by an unknown pathogen. J Neural Transm 110: 517-536.
38. Li JY, Englund E, Holton JL, Soulet D, Hagell P, et al. (2008) Lewy bodies in grafted neurons in subjects with Parkinson's disease suggest host-to-graft disease propagation. Nat Med 14: 501-503.
39. Kordower JH, Chu Y, Hauser RA, Freeman TB, Olanow CW (2008) Lewy body-like pathology in long-term embryonic nigral transplants in Parkinson's disease. Nat Med 14: 504-506.
40. Mendez I, Vinuela A, Astradsson A, Mukhida K, Hallett P, et al. (2008) Dopamine neurons implanted into people with Parkinson's disease survive without pathology for 14 years. Nat Med 14: 507-509.
41. Meyer-Luehmann M, Spires-Jones TL, Prada C, Garcia-Alloza M, de Calignon A, et al. (2008) Rapid appearance and local toxicity of amyloid-beta plaques in a mouse model of Alzheimer's disease. Nature 451: 720-724.
42. Brundin P, Li JY, Holton JL, Lindvall O, Revesz T (2008) Research in motion: the enigma of Parkinson's disease pathology spread. Nat Rev Neurosci 9: 741-745.
43. Rojo AI, Cavada C, de Sagarra MR, Cuadrado A (2007) Chronic inhalation of rotenone or paraquat does not induce Parkinson's disease symptoms in mice or rats. Exp Neurol 208: 120-126.

44. Inden M, Kitamura Y, Takeuchi H, Yanagida T, Takata K, et al. (2007) Neurodegeneration of mouse nigrostriatal dopaminergic system induced by repeated oral administration of rotenone is prevented by 4-phenylbutyrate, a chemical chaperone. J Neurochem 101: 1491-1504.
45. Seehafer SS, Pearce DA (2006) You say lipofuscin, we say ceroid: defining autofluorescent storage material. Neurobiol Aging 27: 576-588.
46. Sherer TB, Betarbet R, Testa CM, Seo BB, Richardson JR, et al. (2003) Mechanism of toxicity in rotenone models of Parkinson's disease. J Neurosci 23: 10756-10764.
47. Betarbet R, Sherer TB, MacKenzie G, Garcia-Osuna M, Panov AV, et al. (2000) Chronic systemic pesticide exposure reproduces features of Parkinson's disease. Nat Neurosci 3: 1301-1306.
48. Hoglinger GU, Lannuzel A, Khondiker ME, Michel PP, Duyckaerts C, et al. (2005) The mitochondrial complex I inhibitor rotenone triggers a cerebral tauopathy. J Neurochem 95: 930-939.
49. Huang J, Liu H, Gu W, Yan Z, Xu Z, et al. (2006) A delivery strategy for rotenone microspheres in an animal model of Parkinson's disease. Biomaterials 27: 937-946.
50. Tofaris GK, Garcia Reitbock P, Humby T, Lambourne SL, O'Connell M, et al. (2006) Pathological changes in dopaminergic nerve cells of the substantia nigra and olfactory bulb in mice transgenic for truncated human alpha-synuclein(1-120): implications for Lewy body disorders. J Neurosci 26: 3942-3950.
51. Gundersen HJ, Bendtsen TF, Korbo L, Marcussen N, Moller A, et al. (1988) Some new, simple and efficient stereological methods and their use in pathological research and diagnosis. Apmis 96: 379-394.
52. West MJ, Slomianka L, Gundersen HJ (1991) Unbiased stereological estimation of the total number of neurons in thesubdivisions of the rat hippocampus using the optical fractionator. Anat Rec 231: 482-497.

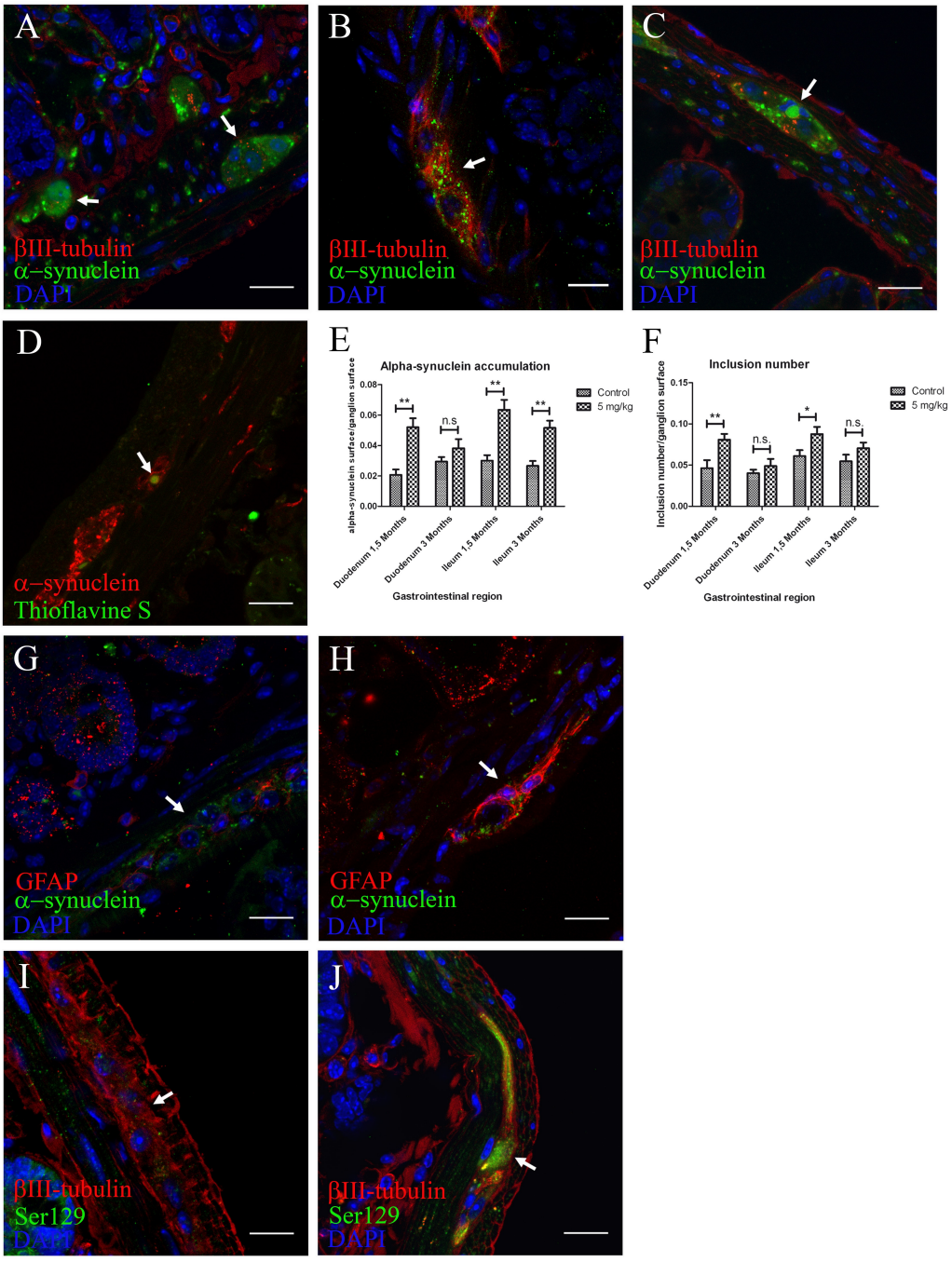

Figure 1. Locally administered rotenone induces alpha-synuclein phosphorylation, accumulation and aggregation with gliosis in ENS ganglia. (scale bars 20 μm). **a**, **b**, **c**,

anti ßIII-tubulin, alpha-synuclein and DAPI staining in duodenum (**b**) and ileum (**a**,**c**) sections. Arrow in **b**, 1.5 months treatment induced an increased alpha-synuclein punctate pattern inside enteric nervous system ganglia when compared to 3 months controls (**a**). Arrow in **c**, 3 months treatment induced formation of larger alpha-synuclein inclusions (>6 µm). **d**, staining using anti-alpha-synuclein, Thioflavine S and DAPI. Arrow in **d**, only 3 months treated mice showed aggregation of these larger alpha-synuclein accumulations. **e**, **f**, quantification of the experiment shown in **a**-**c** was made using automatic segmentation and entropy-based thresholding methods. Single-asterisk, $P<0.05$, and double-asterisk, $P<0.01$. **e**, each column represents total alpha-synuclein surface/ganglion surface. **f**, each column represents total number of alpha-synuclein inclusions/ganglion surface. All graphs show mean ± s.e.m.. **g**, **h**, max-projection of staining against GFAP, alpha-synuclein and DAPI on duodenum sections from control (**g**) and treated (**h**) mice. **i**, **j**, max-projection of anti-ßIII-tubulin, anti-phospho-alpha-synuclein (Ser 129) and DAPI staining on duodenum sections from control (**i**) and treated (**j**) animals

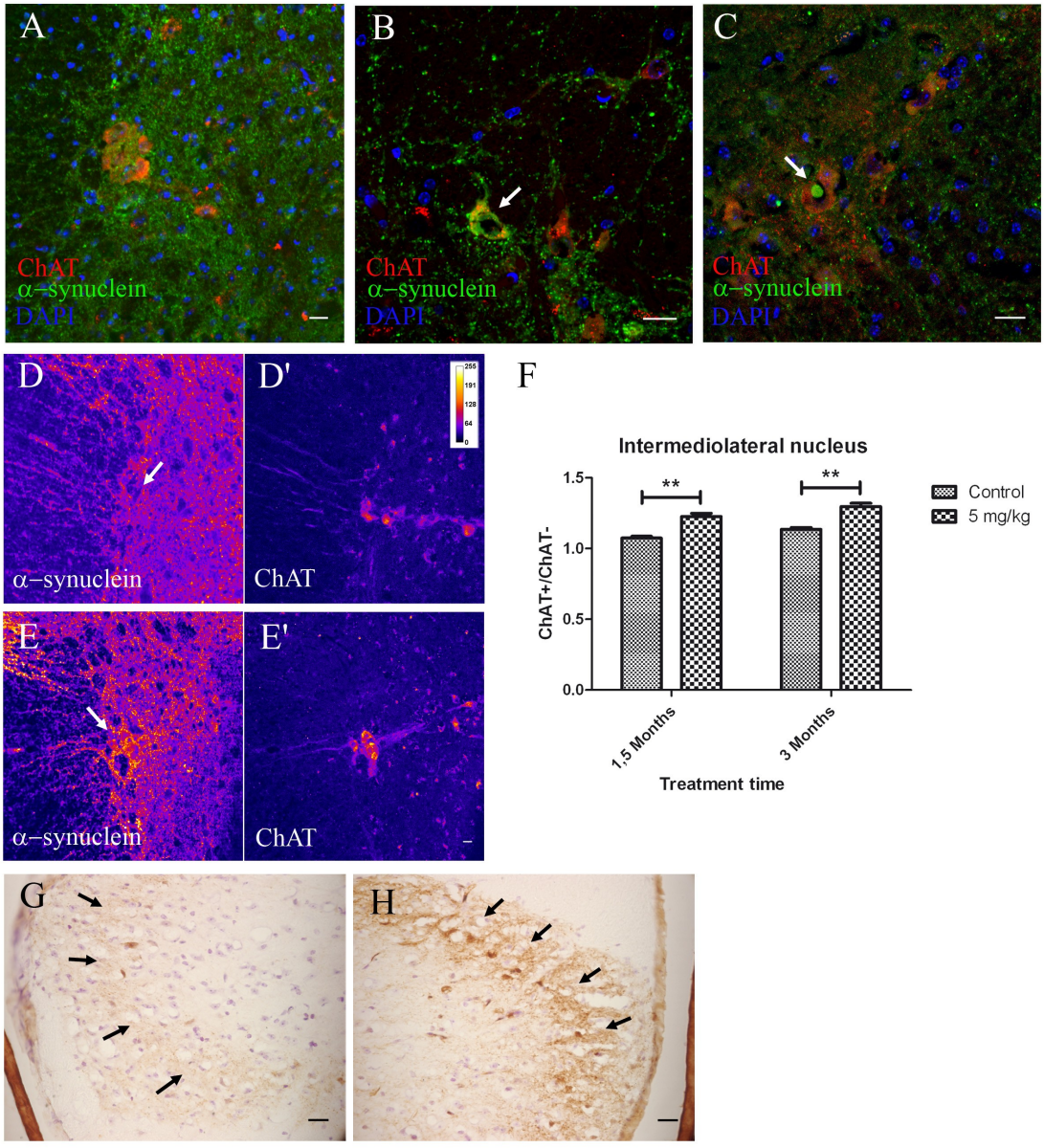

Figure 2. Intracellular and axonal alpha-synuclein increases in the intermediolateral nucleus and the dorsal horn lamina I layer of the spinal cord after oral rotenone treatment. (scale bars 20 µm) **a**, **b**, **c**, Immunostaining against alpha-synuclein and choline acetyl transferase (ChAT) in spinal cord sections showing the intermediolateral nucleus $ChAT^+$ neurons from 3 months control mice (**a**), 1.5 months (**b**) and 3 months (**c**) treated mice. Arrow in **b**, colocalization of increased intracellular alpha-synuclein and $ChAT^+$ stainings in the IML. Arrow in **c**, large alpha-synuclein inclusion (>7.5 µm) inside an IML $ChAT^+$ neuron. **d**-**e**, fluorescence intensity color-coded images from 3 months control (**d, d'**) and 3 months treated mice (**e, e'**) spinal cord sections stained using DAPI and alpha-synuclein and ChAT antibodies. Arrows in **d** and **e**, areas in the proximity of $ChAT^+$ neurons. **f**, mean fluorescence quantification of experiment shown in **d** and **e**. Double asterisk , P<0,01. Columns represent mean alpha-synuclein fluorescence in and around $ChAT^+$ neurons in the IML/ mean alpha-synuclein fluorescence in the region anterior to the IML. Graph shows mean ± s.e.m.. **g**, **h**, DAB-staining against apha-synuclein using synuclein-1 antibody in the dorsal horn of the spinal cord from 3 months treated (**h**) and control (**g**) mice. Arrows in **g**-**h**, lamina I layer of the dorsal horn.

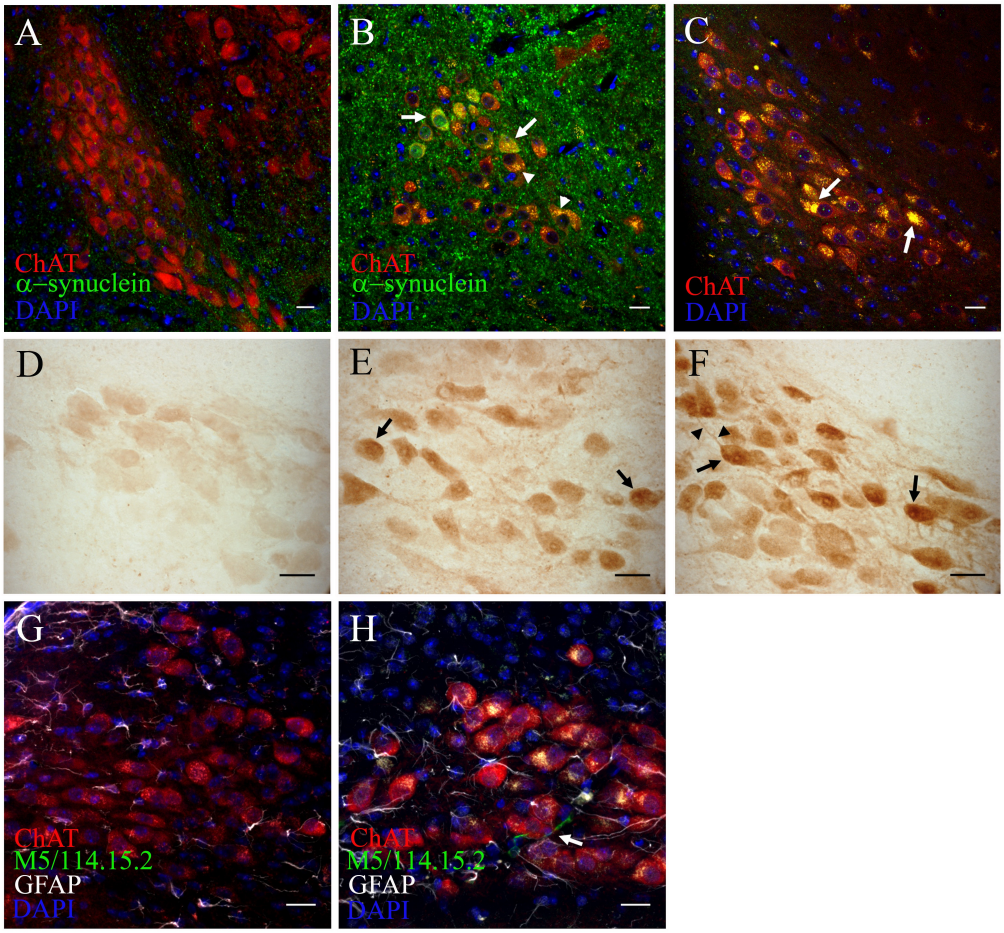

Figure 3. Intragastrically administered rotenone induces alpha-synuclein accumulation, oxidative stress and inflammation in the dorsal motor nucleus vagus.

(scale bars 20 µm). **a**, **b**, double-immunofluorescence staining against alpha-synuclein and ChAT on DMV sections from 1.5 months control (**a**) and 1.5 months treated (**b**) mice. Arrows in **b**, increased intracellular alpha-synuclein in DMV neurons already after 1.5 months. Arrowheads in **b**, autofluorescent punctate inclusion pattern inside $ChAT^+$ neurons. **c**, DMV sections stained with ChAT and DAPI were sequentially excited with 488 and 561 laser wavelengths. Arrows in **c**, large intracellular auto-fluorescent inclusions inside $ChAT^+$ neurons of the DMV (arrows). **d**, **e**, **f**, Light microscopy images of alpha-synuclein staining from 1.5 months control (**d**), 1.5 months (**e**) and 3 months (**f**) treated mice. Arrows in **e** and **f**, increased staining intensity inside DMV neuronal soma in treated mice. Arrowheads in **f**, increased alpha-synuclein staining inside neuronal processes **g**, **h**, average-projection of triple-immunofluorescence staining against ChAT, GFAP, MHC II (clone M5/114.15.2) and DAPI on sections from control (**g**) and treated (**h**) mice. Arrow in **h**, activated microglial cell in the DMV.

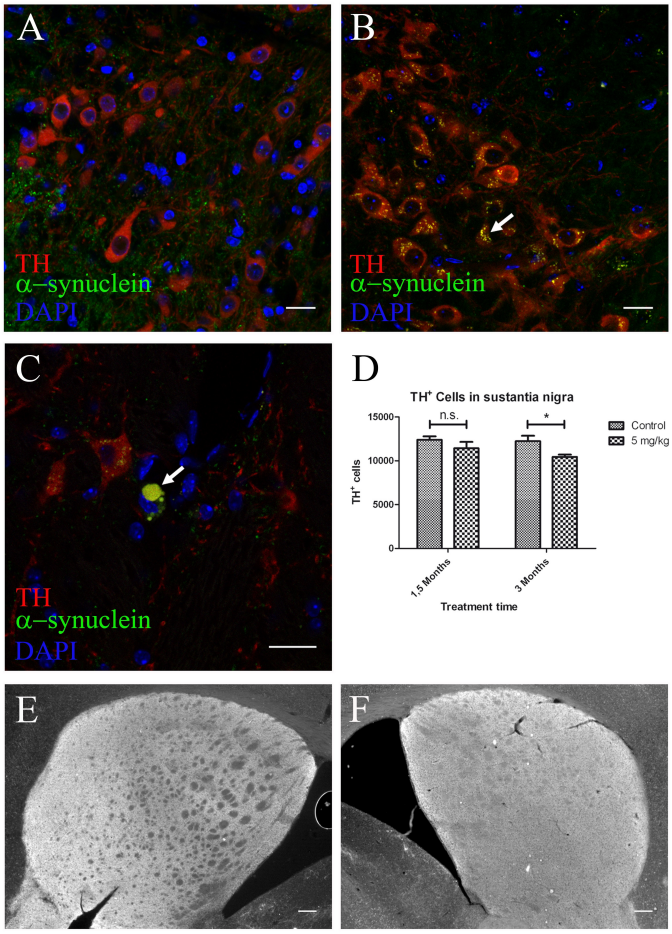

Figure 4. Alpha-synuclein accumulation and neuronal loss in the SN after 3 but not 1.5 months intragastrical rotenone treatment. (**a-c**, scale bars 20 µm; **e-f**, scale bars

200 µm). **a**, **b**, **c**, immunostaining against TH, alpha-synuclein and DAPI on SNc sections from 1.5 months control (**a**) and 3 months (**b**-**c**) treated mice. Arrow in **b**, alpha-synuclein small inclusions inside TH^+ neurons. Arrow in **c**, large alpha-synuclein inclusion (>8.14 µm) inside a dopamineric neuron in the SN. **d**, stereological quantification (n=3) of TH^+ neurons in the SN from control and treated mice. Asterisk, $P<0.05$. Number of neurons was determined based on the optical fractionator principle using StereoInvestigator software (MicroBrightField Inc., Williston, USA). Each column represents total number of TH^+ neurons in the SN in 1.5 and 3 months control and treated mice. Graph shows mean ± s.e.m.. **e**, **f**, TH immunostaining on striatum in 1.5 months control (**e**) and 3 months treated (**f**) mice.

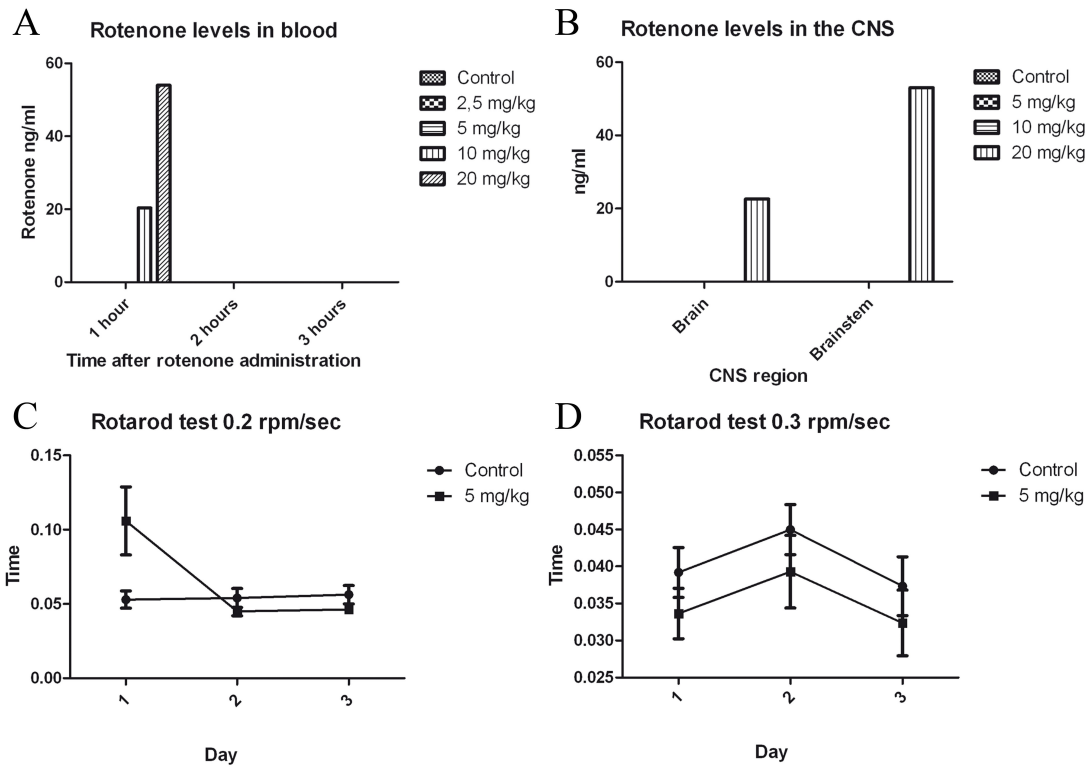

Supplementary figure 1. Motor dysfunctions on rotenone treated mice without detection of rotenone in blood or CNS. a, **b**, quantification of rotenone levels in blood

(**a**) and CNS (**b**). **a**, blood levels 1, 2 and 3 hours after treatment. Mice were divided in three groups (n=3) and treated with 2.5, 5, 10 and 20 mg/kg rotenone (n=3), 300 µl of blood was extracted 1, 2 and 3 hours after rotenone administration and pooled together for HPLC analysis. **b**, mice were treated for one week once a day with 5 (n=3), 10 (n=3) and 20 (n=1) mg/kg rotenone, brain and brainstem were extracted 1 and 2 hours after last administration and prepared for HPLC analysis. **c**, **d**, acceleration protocols using 0.2 rpm/sec (**c**) and 0.3 rpm/sec (**d**) acceleration rates of the rotarod test performed on 3 months treated mice. P is <0.05, values based on Student's t test. All error bars correspond to ± s.e.m..

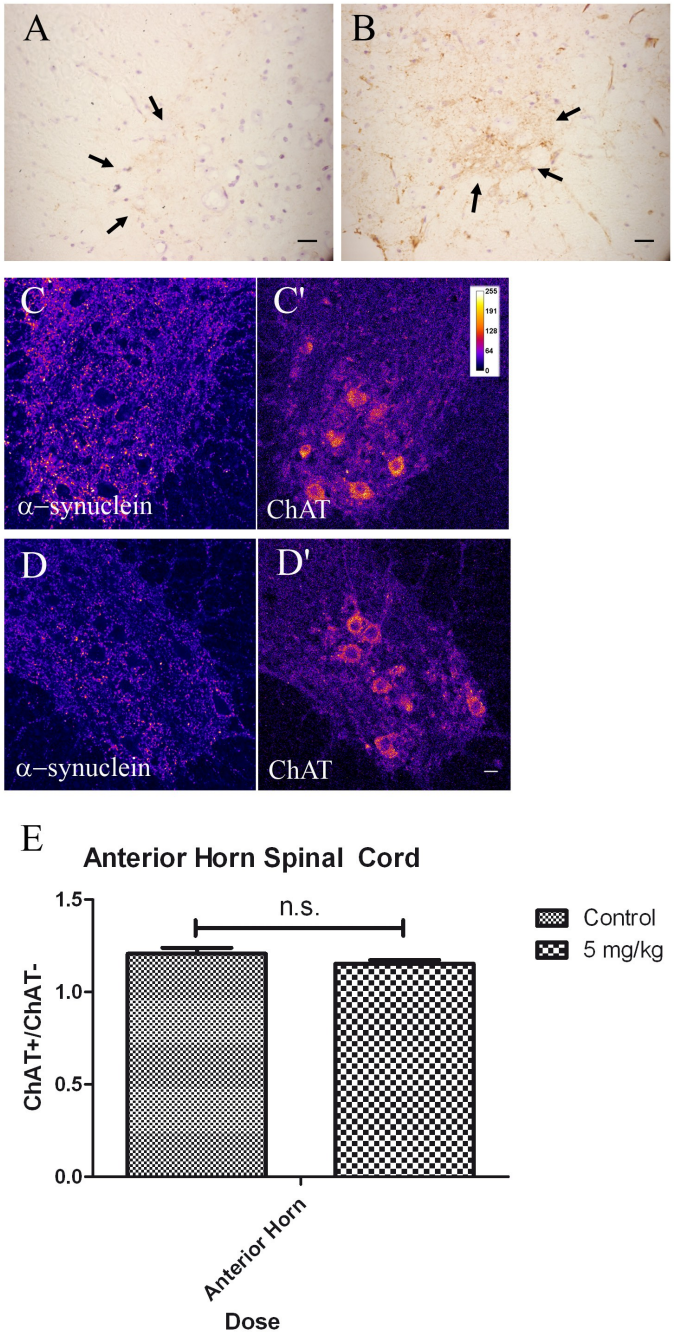

Supplementary figure 2. Rotenone administered orally induces alpha-synuclein accumulation in the IML but not in the motor neurons from the anterior horn of the

spinal cord. (scale bars 20 µm). **a**, **b**, DAB stained spinal cord sections counterstained with cresyle violet from control (**a**) and treated mice (**b**). Arrows in **a** and **b**, IML region of the spinal cord. **c**, **d**, fluorescence intensity color-coded images of $ChAT^+$ motor neurons of the anterior horn from control (**c**) and treated (**d**) mice. **e**, mean fluorescence quantification of experiment shown in **c** and **d**. Columns represent mean alpha-synuclein fluorescence in and around $ChAT^+$ neurons in the anterior horn/ mean alpha-synuclein fluorescence in the region posterior to the motor neurons. Graph shows mean ± s.e.m..